nature structural & molecular biology

Mechanistic basis for the recognition of a misfolded protein by the molecular chaperone Hsp90

Javier Oroz[1,4], Jin Hae Kim[1,4], Bliss J Chang[2] & Markus Zweckstetter[1–3]

The critical toxic species in over 40 human diseases are misfolded proteins. Their interaction with molecular chaperones such as Hsp90, which preferentially interacts with metastable proteins, is essential for the blocking of disease progression. Here we used nuclear magnetic resonance (NMR) spectroscopy to determine the three-dimensional structure of the misfolded cytotoxic monomer of the amyloidogenic human protein transthyretin, which is characterized by the release of the C-terminal β-strand and perturbations of the A-B loop. The misfolded transthyretin monomer, but not the wild-type protein, binds to human Hsp90. In the bound state, the Hsp90 dimer predominantly populates an open conformation, and transthyretin retains its globular structure. The interaction surface for the transthyretin monomer comprises the N-terminal and middle domains of Hsp90 and overlaps with that of the Alzheimer's-disease-related protein tau. Taken together, the data suggest that Hsp90 uses a mechanism for the recognition of aggregation-prone proteins that is largely distinct from those of other Hsp90 clients.

A large number of diseases have been linked to the incorrect folding and aggregation of proteins, with the most toxic species being misfolded proteins[1,2]. Disease progression is critically influenced by the interaction of these incorrectly folded proteins with the molecular chaperones Hsp70 and Hsp90, because molecular chaperones select proteins for refolding or elimination[3–7]. Hsp90 is a key regulator in this process, because it preferentially interacts with unstable proteins[8,9]. However, little is known about how Hsp90 interacts with misfolded proteins, which structural motifs are recognized in the incorrectly folded protein, and how these factors affect the structure of both the substrate and Hsp90.

Hsp90 interacts with a variety of structurally diverse client proteins, including kinases and intrinsically disordered proteins[10–13]. In agreement with its important role in amyloid diseases, Hsp90 binds to the Parkinson's-disease-related protein α-synuclein and influences its aggregation and vesicle interaction[14]. In addition, the disease-associated proteins tau and transthyretin (TTR) interact with Hsp90 (refs. 12,15,16). TTR, which aggregates into insoluble deposits in TTR amyloidosis[17], binds to the Hsp90 isoform found in the endoplasmic reticulum (GRP-94), an interaction that is found in the cytosol of pancreatic cells[15]. Moreover, retention of a misfolded form of TTR in the endoplasmic reticulum results in upregulation of GRP-94 (ref. 18), and perturbation of endoplasmic reticulum proteostasis increases the number of extracellular TTR aggregates[19].

TTR deposits are found in the peripheral nervous system and the heart, where they cause neuropathy and cardiomyopathy, respectively[20]. The cardiac form of TTR amyloidosis is more common among people of African ancestry—it affects 3–4% of African Americans. Currently, more than 100 autosomal dominant variants of the *TTR* gene are known[21,22]. In the native state, the 127-residue protein TTR assembles into a 55-kDa homotetrameric structure. Each subunit contains two β-sheets composed of strands D-A-G-H and C-B-E-F[23]. The tetramer is then formed by interactions between the two loops, which connect strands A and B in one molecule and strands G and H in a second molecule. The native tetrameric structure is important for the physiological function of TTR in human plasma, where it transports thyroxine and the holo-retinol-binding protein.

In studies designed to improve the mechanistic understanding of TTR misfolding, researchers have defined more than 200 crystal structures of wild-type and disease-associated mutated TTR[24,25]. All of the crystal structures, however, are highly similar and show the native tetrameric TTR arrangement. Because dissociation of the native homotetrameric protein into a misfolded monomeric state is the key step in the misfolding cascade of TTR[26,27], the structure of the critical misfolded species of TTR has remained enigmatic. Previous studies have shown that the monomeric misfolded form of TTR contains elements of rigid secondary structure[23,28,29] but is more dynamic than the native TTR protein and other native-state clients of Hsp90. Thus, scientists interested in this protein face three critical questions: (i) what is the structure of the misfolded monomeric TTR, (ii) how does it interact with the highly dynamic 167-kDa Hsp90 chaperone and (iii) how does the interaction influence the conformation of both the misfolded protein and Hsp90?

Here we investigated the solution structure of the misfolded monomer of TTR and its interaction with the molecular chaperone Hsp90 at high resolution (**Fig. 1a**). Through a combination of NMR spectroscopy methods optimized for macromolecular machines and small-angle X-ray scattering (SAXS), we identified the structural changes

[1]German Center for Neurodegenerative Diseases (DZNE), Göttingen, Germany. [2]Department for NMR-based Structural Biology, Max Planck Institute for Biophysical Chemistry, Göttingen, Germany. [3]Department of Neurology, University Medical Center Göttingen, University of Göttingen, Göttingen, Germany. [4]These authors contributed equally to this work. Correspondence should be addressed to M.Z. (Markus.Zweckstetter@dzne.de).

Received 23 June 2016; accepted 17 January 2017; published online 20 February 2017; corrected online 13 March 2017; doi:10.1038/nsmb.3380

that occur during misfolding of TTR and the interaction sites in the TTR–Hsp90 complex, and we examined how complex formation influences the structures of the substrate and Hsp90. Our study thus dissects the mechanistic basis for the interaction of a key molecular chaperone with a toxic misfolded protein.

RESULTS

3D structure of the monomeric misfolded state of TTR

To obtain high-resolution insight into the misfolded form of TTR, we examined the cytotoxic TTR variant F87M/L110M (M-TTR)[23,30]. M-TTR crystallizes as a rigid tetramer, whereas in solution the protein is monomeric according to analytical ultracentrifugation, gel filtration analyses[23] and relaxation measurements[29]. Through a variety of multidimensional NMR spectroscopy experiments, we obtained the sequence-specific resonance assignment of the backbone and side chain atoms of M-TTR. Subsequently, we resolved more than 950 medium- and long-range distance restraints and determined the 3D solution structure (**Table 1** and **Supplementary Fig. 1**).

The 3D structure of M-TTR shows that the short α-helix in the E-F loop is only slightly perturbed in the monomeric protein, and the β-sheet formed by strands C, B, E and F is native-like (**Fig. 1b–d**). In contrast, β-strand H is not stably formed (**Fig. 1b**,**d**), in agreement with chemical-shift-derived order parameters (**Fig. 1e**) and relaxation dispersion experiments for M-TTR[29]. Because of the destabilization of β-strand H, the nearby loop connecting β-strands F and G is rotated (**Fig. 1d**). In addition, the conformation of the loop between strands A and B deviates from that observed in the tetrameric protein (**Fig. 1d**). In the tetrameric protein, the A-B loop forms hydrogen bonds with strand H from another subunit and is thus critical for tetramerization[24]. The A-B loop of M-TTR also appears to be more flexible (**Fig. 1e**) than that in the native structure, in agreement with conformational changes in the region of the A-B loop that were previously suggested by both solution and solid-state NMR spectroscopy measurements[28,29]. In contrast, β-strands F (residues 91–97) and C (residues 41–48), which form the edge of the C-B-E-F sheet, are more rigid in the monomeric protein (**Fig. 1e**). The release of β-strand H in M-TTR highlights the importance of β-sheet destabilization for protein misfolding[31].

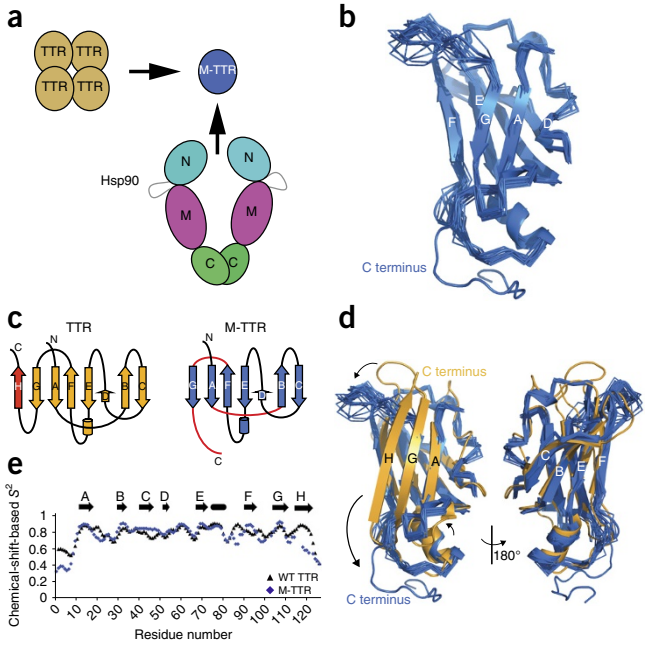

Figure 1 Three-dimensional structure of the cytotoxic conformation of TTR. (**a**) The dissociation of the native homotetrameric protein (gold) into a misfolded monomeric state (blue) is the key step in the misfolding cascade of TTR[26,27]. (**b**) An ensemble of the 20 lowest-energy structures of monomeric misfolded M-TTR. The C-terminal residues, which are disordered in M-TTR but fold into β-strand H in tetrameric TTR, are shown for only one conformer. (**c**) Secondary-structure topology in wild-type TTR (orange) and misfolded M-TTR (blue). β-strand H, which is destabilized in M-TTR (**b**), is shown in red. The A-B and G-F loops of M-TTR are also marked in red. (**d**) Comparison of the misfolded conformation of monomeric TTR (blue) with the structure of a single subunit from tetrameric TTR (orange; PDB 1GKO). Arrows highlight the release of β-strand H and the change in A-B and G-F loop orientation in the monomeric misfolded protein. β-sheets of native TTR are labeled. (**e**) NMR chemical shifts revealed distinct structural flexibilities of the backbone of M-TTR and wild-type (WT) TTR (BMRB 5507; data from ref. 51). The location of β-strands in wild-type TTR is shown at the top.

Hsp90 recognizes misfolded TTR

Because the interaction between misfolded proteins and molecular chaperones is critical for the blocking of disease progression[3–7], we investigated the interaction of M-TTR with Hsp90. We selected the constitutive isoform Hsp90β, which is highly overexpressed in the cytoplasm of eukaryotic cells[32] and for which the interaction with the intrinsically disordered substrate tau has been characterized[16]. We prepared full-length human Hsp90β recombinantly and added it to M-TTR, and we observed the ensuing interaction by NMR spectroscopy. In the two-dimensional ^{1}H-^{15}N correlation spectrum of M-TTR (**Fig. 2a**), we observed one backbone cross-peak for each non-proline residue of M-TTR. After the addition of an equimolar concentration of Hsp90, the

Table 1 NMR spectroscopy and refinement statistics for protein structures

	M-TTR (PDB 2NBO)
NMR distance and dihedral constraints	
Distance constraints	
Total nuclear Overhauser effect	2,037
Intraresidue	461
Inter-residue	
Sequential ($\|i-j\|=1$)	619
Medium-range ($\|i-j\|<4$)	243
Long-range ($\|i-j\|>5$)	714
Intermolecular	
Hydrogen bonds	50
Total dihedral angle restraints	
ϕ	80
ψ	83
Structure statistics	
Violations (mean ± s.d.)	
Distance constraints (Å)	0.01 ± 0.00
Dihedral angle constraints (°)	0.30 ± 0.06
Max. dihedral angle violation (°)	4.06 ± 0.44
Max. distance constraint violation (Å)	0.29 ± 0.01
Deviations from idealized geometry	
Bond lengths (Å)	0.001
Bond angles (°)	0.2
Impropers (°)	0
Average pairwise r.m.s. deviation[a] (Å)[b]	
Heavy	0.9
Backbone	0.4

[a]Pairwise r.m.s. deviation was calculated among 20 refined structures. [b]Residues 10–55, 58–85, 91–98 and 105–112 of M-TTR were considered ordered by the Protein Structure Validation Software Suite.

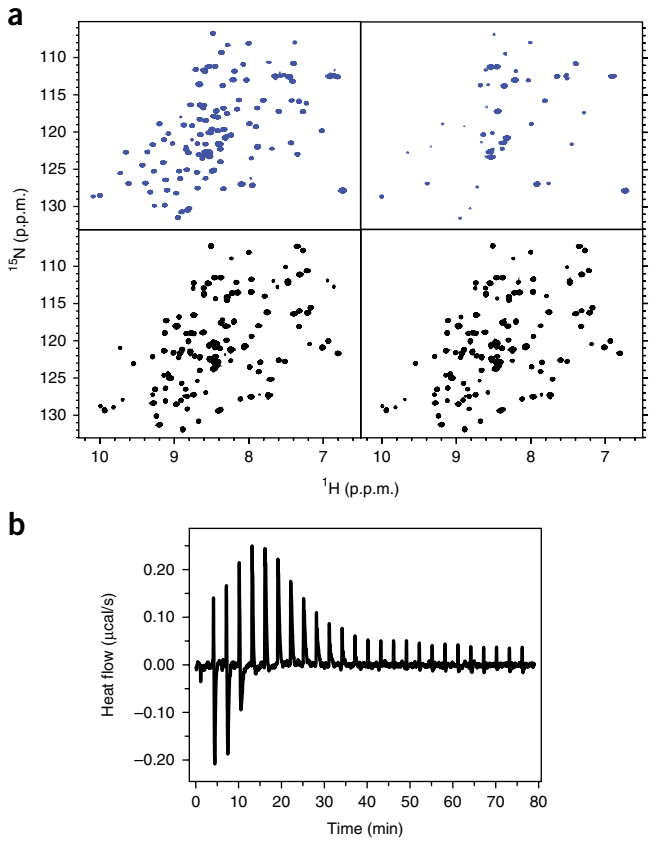

Figure 2 The molecular chaperone Hsp90 binds to misfolded TTR. (**a**) ^{1}H-^{15}N NMR spectra of M-TTR (top, blue; 150 µM protein) but not wild-type TTR (bottom, black; 150 µM protein) were strongly attenuated after the addition of an equimolar amount of 167-kDa Hsp90 (right). The remaining M-TTR peaks (top right) corresponded to residues near the N and C termini of the protein. (**b**) Calorimetric titration of 25 1.5-µl aliquots of 520 µM M-TTR into 113 µM Hsp90.

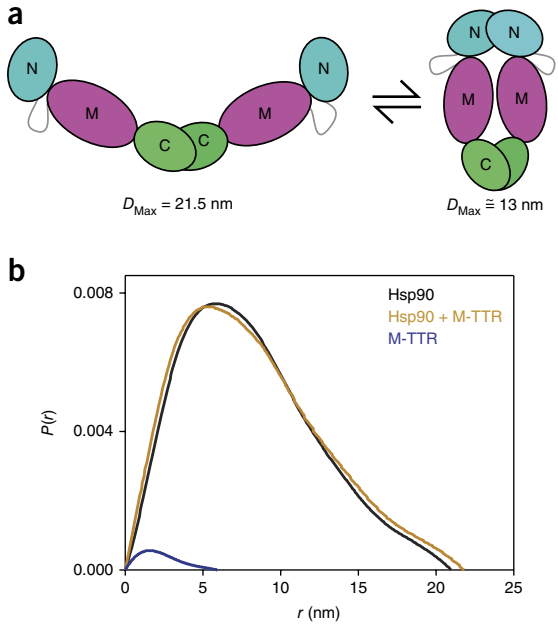

Figure 3 The Hsp90 dimer is in an open conformation in the presence of M-TTR. (**a**) Schematic representation of the dynamic structure of Hsp90, which constantly switches between open and closed states. The maximum dimensions as derived from SAXS (**b** and ref. 35) are indicated. (**b**) Normalized *P*(*r*) SAXS profiles of M-TTR (50 µM), Hsp90 (50 µM) and Hsp90 + M-TTR (2:1 molar ratio, using 50 µM Hsp90). M-TTR is included for comparison and shows R_g = 1.85 ± 0.23 nm and D_{Max} = 6.07 ± 0.33 nm.

NMR signals of most M-TTR residues were strongly attenuated (**Fig. 2a**). In particular, the resonances downfield of 8.5 p.p.m., which are characteristic for β strands, disappeared almost completely. Sequence-specific assignment showed that the remaining signals belonged to the flexible N- and C-terminal residues of M-TTR. The decrease in NMR signal intensity is due to the drastic increase in molecular weight after the 13.8-kDa M-TTR and the 167-kDa chaperone Hsp90 form a complex. A similar attenuation of the NMR signals in two-dimensional ^{1}H-^{15}N correlation spectra was observed for the DNA-binding domain of the tumor suppressor p53 after binding to Hsp90 (ref. 33).

Next we probed the interaction of Hsp90 with wild-type tetrameric TTR (**Fig. 2a**). The NMR spectra of tetrameric TTR in the absence and in the presence of an equimolar amount of Hsp90 were highly similar (**Fig. 2a**). Both rigid and flexible TTR residues fully retained their intensity. The combined data show that Hsp90 binds to the monomeric misfolded form of TTR but not to the native tetrameric structure, in agreement with the preferential interaction of Hsp90 with non-native, metastable proteins[9,10].

The interaction between M-TTR and Hsp90 was further supported by isothermal titration calorimetry (ITC) analysis. The analysis revealed two distinct phases with opposite thermodynamic properties, thus suggesting that multiple binding events were occurring (**Fig. 2b** and **Supplementary Fig. 2**). The highest-affinity binding event involved a negative enthalpy change, indicating an exothermic process followed by a lower-affinity binding process with endothermic properties (**Supplementary Table 1**). The binding constants derived from these measurements were 0.3 µM and 47.3 µM, respectively, in agreement with micromolar binding affinities reported for other Hsp90 substrates[11,16,34,35].

Hsp90 is predominantly in an open conformation in complex

Structural analysis of Hsp90–substrate complexes is technically challenging because of the dynamic nature of Hsp90, the unstable folding of substrates and the complexity of the Hsp90 chaperone cycle. In addition, the micromolar concentration range for the binding of many Hsp90 substrates precludes analysis by electron microscopy[11]. We therefore used SAXS to investigate the consequences of M-TTR binding for the Hsp90 structure. SAXS has been shown to be a powerful tool for mapping the dynamic ensemble of Hsp90 conformations[36] in which the Hsp90 dimer switches between open and closed forms (**Fig. 3a**).

We used experimental X-ray scattering intensities to derive the interatomic-distance distribution of full-length human Hsp90 (**Fig. 3b**). Interatomic distances reached up to ~21.5 nm (radius of gyration (R_g) = 6.43 ± 0.17 nm, and maximum particle size (D_{Max}) = 21.52 ± 0.99 nm), thus indicating the presence of a substantial amount of open-state Hsp90 dimer. In the presence of M-TTR, the maximum of the *P*(*r*) distribution remained largely unchanged. Only the largest value of the derived interatomic distances increased to ~22 nm (R_g = 6.54 ± 0.05 nm, D_{Max} = 22.22 ± 0.37 nm; **Fig. 3b**), which is consistent with binding of M-TTR to Hsp90. We obtained similar results when we repeated the experiment in the presence of ADP (**Supplementary Fig. 3**), which suggests that ADP does not promote allosteric changes in the Hsp90–M-TTR complex. Therefore the SAXS results show that the Hsp90 dimer populates a predominantly open conformation in the presence of the misfolded M-TTR protein.

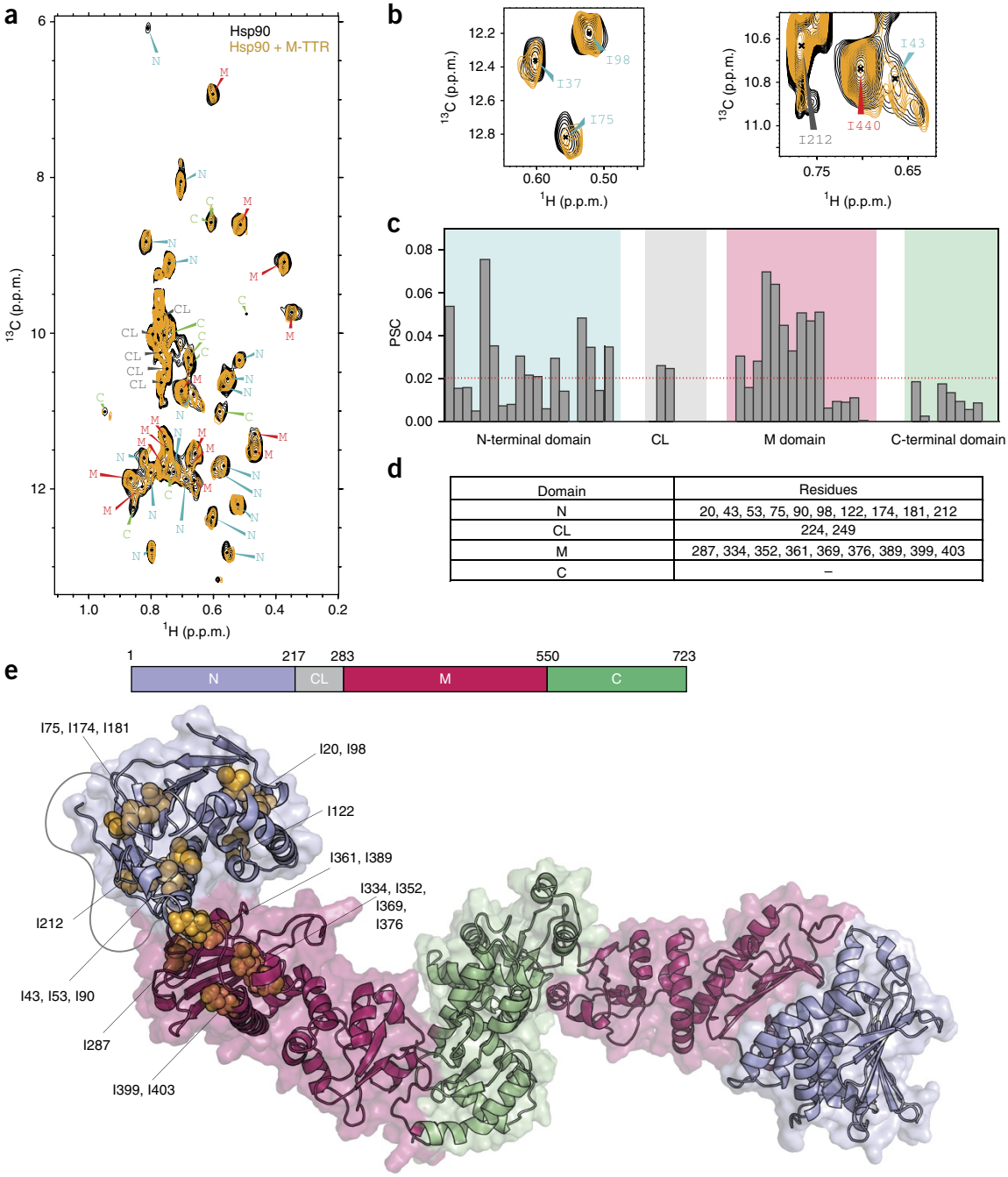

Domain	Residues
N	20, 43, 53, 75, 90, 98, 122, 174, 181, 212
CL	224, 249
M	287, 334, 352, 361, 369, 376, 389, 399, 403
C	–

Figure 4 The metastable monomeric variant of TTR binds to the N-terminal and M domains of Hsp90. (**a**,**b**) Methyl-TROSY spectra of full-length isoleucine-labeled Hsp90 (80 μM protein) and Hsp90–M-TTR complex (Hsp90:M-TTR molar ratio of 1:4). Isoleucine residues in the N-terminal, M and C-terminal domains of Hsp90 are labeled in cyan, red and green, respectively; charged linker (CL) resonances are shown in gray. (**c**) PCSs on Hsp90 isoleucine methyl groups induced upon interaction with lanthanide-tagged M-TTR. (**d**,**e**) Identification of the M-TTR binding site in full-length Hsp90 by PCS (**c**). Residues with PCSs greater than 0.02 (red dotted line in **c**) are listed in **d** and marked by orange spheres in **e**. All affected isoleucine moieties are located in the N-terminal and M domains. Affected residues that belong to the CL are not marked in the structure in **e**. The charged linker, which connects Hsp90's N-terminal and M domains, is represented by a gray line in **e**.

Hsp90 N-terminal and middle domains interact with monomeric TTR

Despite the wide range of available Hsp90 substrates, little is known about where and how substrates bind to Hsp90. In particular, the binding of a misfolded protein intermediate to this homodimeric 167-kDa molecular chaperone, and thus a critical step in the development of amyloid diseases, has remained elusive. This is due to the high molecular weight of Hsp90 and its extensive interdomain dynamics. To identify the binding site of M-TTR on full-length Hsp90, we specifically labeled the methyl groups of Hsp90 isoleucine residues, which are well spread over the Hsp90 structure[16,37] (**Fig. 4a**). Through this labeling approach, single residues can be observed by NMR spectroscopy in high-molecular-weight complexes[38]. The two-dimensional ^{1}H-^{13}C TROSY spectrum of the full-length Hsp90 dimer, in which

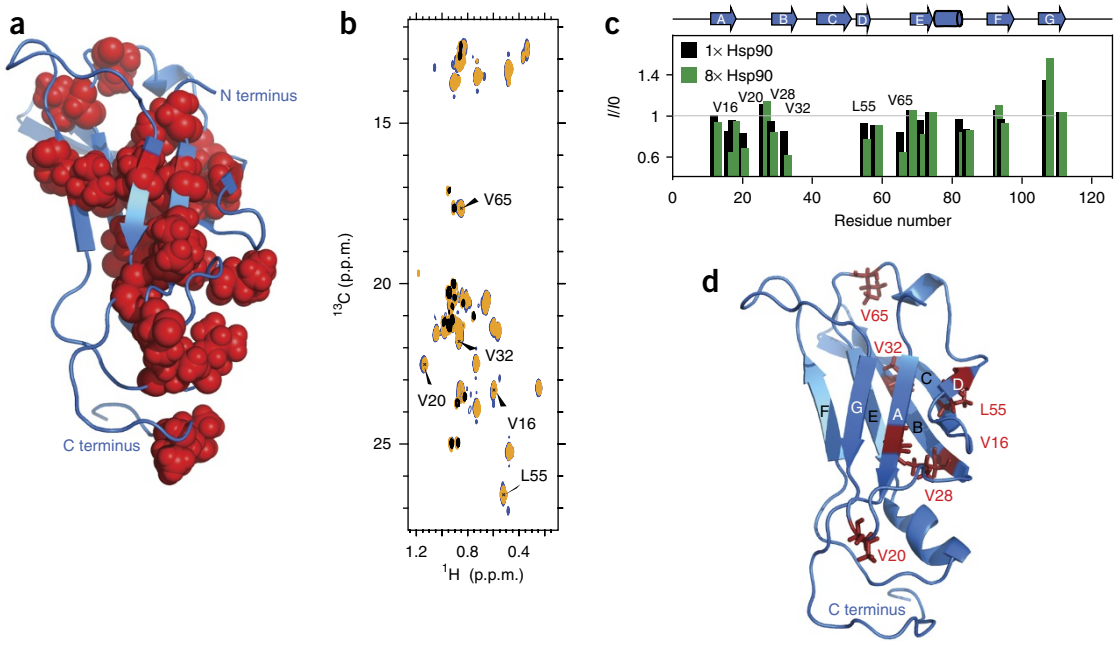

Figure 5 TTR retains its globular structure in complex with Hsp90. (**a**) Methyl groups of leucine, valine and isoleucine residues (shown as red spheres) are distributed across the TTR structure. (**b**) Methyl-TROSY spectra of M-TTR in the absence (blue; 150 μM protein) and presence of a four-fold molar excess of Hsp90 (orange). Comparison with a natural-abundance spectrum of Hsp90 alone (black; 250 μM) shows that the additional sharp peaks originate from Hsp90. (**c**,**d**) Residue-specific changes in the intensity (**c**) of methyl signals of M-TTR with increasing concentrations of Hsp90 (black, equimolar (1×) concentration of M-TTR and Hsp90; green, eight-fold molar excess of Hsp90). The side chains of the most strongly broadened residues are marked in the structure of M-TTR (**d**).

the methyl groups of isoleucine residues were protonated in a fully deuterated background, revealed well-resolved signals (**Fig. 4a**). Defined cross-peaks from all three domains of Hsp90—the N-terminal domain, the middle (M) domain and the C-terminal dimerization domain—were identified and were largely consistent with previous results[37]. The addition of increasing amounts of M-TTR caused changes in the positions and intensities of a small number of Hsp90 signals, which indicated that the exchange rate between the bound and free forms is intermediate to slow on the NMR time scale (**Fig. 4a**,**b**). As most of the signals remained unperturbed, the spectra demonstrate that the three Hsp90 domains retain their internal structure when M-TTR binds to Hsp90. Further analysis showed that the perturbed Hsp90 residues belong primarily to the N-terminal domain, with additional changes in the M domain (**Fig. 4b**).

Because chemical shifts are sensitive to both binding events and structural changes, we sought to obtain direct support for the Hsp90-M-TTR interaction interface. To this end, we introduced a second cysteine at position 13 (the M13C mutation, close to the native cysteine at position 10) in M-TTR and covalently labeled the protein with the CLaNP-7 lanthanide tag, which carried either a paramagnetic Tm^{3+} or a diamagnetic Lu^{3+} ion[39,40]. The advantage of lanthanide tags is that they can induce chemical shift perturbations (pseudocontact shifts (PCSs)) for residues that are spatially close to protein-protein interfaces[41,42]. We identified PCSs for several residues in the N-terminal and M domains of Hsp90, but not in the C-terminal dimerization domain, in agreement with the chemical shift changes observed in the presence of the diamagnetic M-TTR (**Fig. 4b**,**c**). Consistent with the notion of multiple binding sites suggested by the ITC experiments (**Fig. 2b** and **Supplementary Fig. 2**), the most strongly affected residues were located in at least two distinct regions of the Hsp90 structure (**Fig. 4d**,**e** and **Supplementary Fig. 4**).

Structure of monomeric TTR in complex with Hsp90

Next we asked whether we could obtain insight into the 3D structure of M-TTR when it is bound to Hsp90. Because of the high molecular weight of the complex, we used the strategy of selective labeling of methyl groups in a fully deuterated background, which had been successfully applied to Hsp90 (**Fig. 4**). For optimal coverage of the M-TTR structure, we protonated isoleucine, valine and leucine methyl groups, generating 22 methyl groups in total (**Fig. 5a**). We then recorded high-resolution ^{1}H-^{13}C TROSY spectra at increasing concentrations of unlabeled Hsp90 (**Fig. 5b**). In contrast to the severe line broadening that we observed for the backbone resonances of M-TTR after the addition of an equimolar amount of Hsp90 (**Fig. 2a**), we obtained high-quality methyl spectra at up to an eight-fold excess of Hsp90 (**Fig. 5b**). This indicates that the line broadening of the backbone resonances of M-TTR was caused by rapid spin relaxation, a direct consequence of the drastically increased molecular weight after complex formation. In contrast, the methyl groups of M-TTR retained a high degree of flexibility.

A comparison of the methyl TROSY spectra of M-TTR in the absence and in the presence of an eight-fold excess of Hsp90 showed that the position of the cross-peaks remained largely unaffected (**Fig. 5b**). Instead, a selected number of signals were attenuated, in particular those belonging to Val16, Val20, Val28, Val32, Leu55 and Val65 (**Fig. 5c**). These residues are located primarily on the side of M-TTR, which is formed by β-strand A, the A-B loop, strand B and β-strand D (**Fig. 5d**). At the same time, the NMR signal of Ile107, which is located in β-strand G, increased in intensity, thus suggesting that Ile107 becomes more flexible after M-TTR-Hsp90 interaction. Notably, ADP did not modulate the NMR spectra of M-TTR in the presence of Hsp90 (**Supplementary Fig. 3b**), which indicates that the nucleotide state of Hsp90 is not critical for the M-TTR-Hsp90 interaction. The data demonstrate that M-TTR retains its globular structure

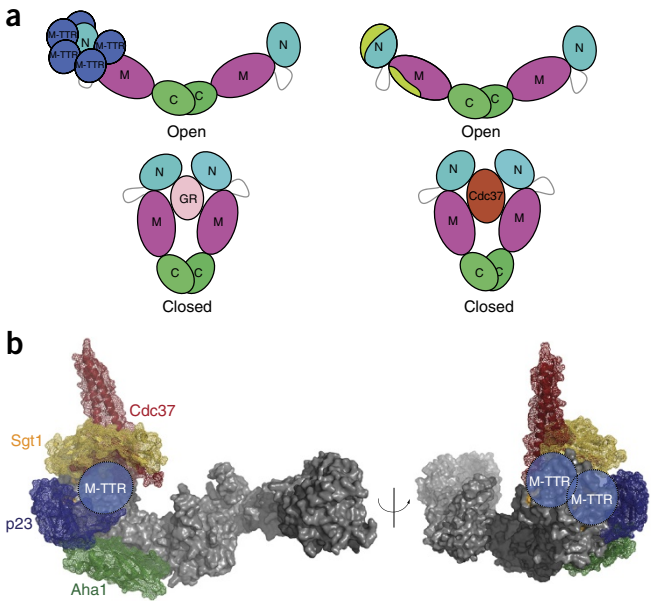

Figure 6 The intrinsically disordered protein tau and the toxic misfolded conformation of TTR share a common binding surface on Hsp90. (**a**) Schematic illustration of Hsp90 binding interfaces with different substrates: M-TTR (blue), intrinsically disordered protein tau (yellow-green)[16], the stabilized ligand-binding domain of the GR (pink)[35] and the co-chaperone Cdc37 (red)[44,46]. Yellow-green shading in the upper-right illustration indicates tau binding. (**b**) Binding of M-TTR does not overlap with Hsp90 interaction sites of the co-chaperones Cdc37, Sgt1, p23 and Aha1 (refs. 44,46–49). The Hsp90 dimer is represented in gray.

after binding to Hsp90. Interaction with Hsp90, however, changes the internal dynamics of the substrate, in particular in the region of TTR, which is buried in the native homotetramer.

DISCUSSION

The molecular chaperone Hsp90 preferentially interacts with metastable proteins[8,9], but it also has a number of client proteins such as kinases, which have a stable 3D structure[43,44]. Our study showed that only the monomeric misfolded form of TTR, and not the native tetrameric protein, is able to bind to Hsp90 with nanomolar to micromolar affinity (**Fig. 2**). Dissociation of native tetrameric TTR into a monomeric state is thus a critical step that enables the protein to be recognized by Hsp90. In addition, the release of β-strand H in M-TTR (**Fig. 1**) exposes hydrophobic residues and thereby further influences the binding to Hsp90. Consistent with these biophysical results, the endoplasmic reticulum quality control system was shown to differentially regulate the fates of wild-type TTR and monomeric misfolded M-TTR[18]. Most of the current therapeutic approaches designed to block TTR aggregation in TTR-related diseases are based on the reported structural information for tetrameric TTR[45]. The atomic structure of the misfolded cytotoxic TTR reported in this work opens the door to the development of small molecules that selectively target TTR's misfolded species. Efforts to target the structure of monomeric, misfolded TTR would constitute a new strategy—one that might interfere less with TTR's physiological functions.

Little is known about the structure of substrates in complex with Hsp90. For example, different reports have suggested that the Hsp90 substrate p53 adopts a molten-globule-like state in the presence of Hsp90 (ref. 33) and that it retains a native-like conformation in complex[34]. It is likely that tau binds Hsp90 in an extended state[16], but the detailed structure of Hsp90-bound tau is currently not known. By using NMR spectroscopy methods optimized for macromolecular machines[38], we observed that that binding of Hsp90 to M-TTR does not perturb the conformation of M-TTR's C-B-E-F sheet or D-A-G β-sheet. In addition, we could not find any evidence that β-strand H was stabilized after binding to Hsp90. Instead, the effects of Hsp90 on the NMR spectra of M-TTR suggested that in the presence of Hsp90 the internal dynamics of M-TTR were changed. Binding of Hsp90 to monomeric TTR might therefore be connected not to TTR refolding but to degradation, in agreement with the finding that the retention of M-TTR in the endoplasmic reticulum induces the unfolded protein response[18].

Substrate binding can modulate the structure of Hsp90 and thus influence its function. Because of the dynamic nature of the Hsp90 dimer, insight into this subject requires approaches that are applicable to dynamic structures in solution, such as SAXS. SAXS has been applied to the Hsp90 dimer[36] and revealed a shift from the open to the closed state upon binding of p23 (ref. 35). In addition, binding of a largely unfolded fragment of staphylococcal nuclease to Hsp90 resulted in partial closure of the Hsp90 dimer[11]. Here we have demonstrated that M-TTR does not induce Hsp90 closure; in fact, Hsp90 remained in a predominantly open conformation in the presence of M-TTR (**Fig. 3b** and **Supplementary Fig. 3**). This finding is consistent with studies of Hsp90 binding to tau, which also does not shift the conformational equilibrium of Hsp90 toward more closed states[16]. A further consequence of a predominantly open Hsp90 conformation in the presence of M-TTR (and tau) is that co-chaperones can readily bind to the substrate–Hsp90 complex.

We hypothesize that the distinct effects of substrates on the structure and function of Hsp90 are related to dedicated interaction surfaces. To support this hypothesis, we compared the Hsp90 interfaces with the kinase Cdc37 (refs. 44,46), a stabilized ligand-binding domain of the glucocorticoid receptor (GR)[35] and the intrinsically disordered protein tau[16] (**Fig. 6a**). We also examined the binding of M-TTR to the N-terminal and M domains of Hsp90. Our first observation was that both the stabilized ligand-binding domain of the GR and the co-chaperone Cdc37 bound to Hsp90 sites that are distinct or only partially overlap with that used for M-TTR binding[35,46]. In contrast, recognition of the aggregation-prone proteins tau and M-TTR by Hsp90 involved similar sites in the N-terminal and M domains of Hsp90. In the case of tau, such a large interaction surface is required in order to enable many low-affinity contacts[16]. In contrast, M-TTR retained a globular structure in complex with Hsp90 (**Fig. 5**), and thus a much smaller Hsp90 region should be sufficient for binding of M-TTR. The observation that M-TTR induced paramagnetic effects in residues, distributed over a broad region involving both the N-terminal and the M domain of Hsp90, indicates that M-TTR binds in multiple Hsp90 sites in a dynamic manner.

In addition to the variations in the regions that Hsp90 uses to recognize different substrates, the global structure of Hsp90 is also affected in distinct ways by these substrates (**Fig. 6a**). Whereas both the stabilized GR ligand-binding domain and Cdc37 shift Hsp90 to partially closed states, Hsp90 remains in an open conformation in the presence of tau and M-TTR. Because Hsp90's structure is tightly linked to its function, the different substrate-binding modes indicate that Hsp90 might use distinct mechanisms when it is involved in regulating protein misfolding versus when it interacts with clients whose *in vivo* function depends on Hsp90. Moreover, the binding of M-TTR to Hsp90 is compatible with the simultaneous binding of co-chaperones[44,46–49] (**Fig. 6b**). Co-chaperones in M-TTR–Hsp90–co-chaperone ternary complexes might thus influence the structure as well as the structural stability of misfolded clients bound to Hsp90, and thereby determine their fate in the cell.

Taken together, our findings provide support for the idea of Hsp90 as an attractive target for the therapeutic treatment of diseases rooted in protein misfolding[50].

METHODS

Methods, including statements of data availability and any associated accession codes and references, are available in the online version of the paper.

Note: Any Supplementary Information and Source Data files are available in the online version of the paper.

ACKNOWLEDGMENTS

We thank M. Mizuguchi (University of Toyama, Toyama, Japan) for the transthyretin plasmid; C.A. Dickey (University of South Florida, Tampa, Florida, USA) for the Hsp90 plasmid; and C.A. Dickey, B.A. Nordhues and S.G. Rüdiger for useful discussions. We are grateful to M. Ubbink (Leiden University, Leiden, the Netherlands) for the CLanP-7 lanthanide tag, to P. Wysoczanski for help with NMR spectroscopy experiments recorded for Hsp90's M domain, and to A. Pérez-Lara for help with ITC experiments. This work was supported by the Alexander von Humboldt Foundation (fellowship to J.H.K.), the European Commission (Marie Curie Intra-European fellowship, project number 626526 to J.O.), the Fulbright Program (scholarship to B.J.C.) and the European Community's Seventh Framework Programme (FP7/2007-2013) under BioStruct-X (grant agreement 283570 to M.Z.).

AUTHOR CONTRIBUTIONS

J.H.K. performed NMR spectroscopy and biochemical experiments on TTR variants, as well as structure calculations. J.O. performed NMR spectroscopy, SAXS and ITC experiments on Hsp90. B.J.C. and J.O. produced Hsp90 mutants for the assignment of isoleucine methyl groups. J.H.K., J.O. and M.Z. designed experiments. J.H.K., J.O. and M.Z. wrote the paper.

COMPETING FINANCIAL INTERESTS

The authors declare no competing financial interests.

1. Haass, C. & Selkoe, D.J. Soluble protein oligomers in neurodegeneration: lessons from the Alzheimer's amyloid β-peptide. *Nat. Rev. Mol. Cell Biol.* **8**, 101–112 (2007).
2. Chiti, F. & Dobson, C.M. Protein misfolding, functional amyloid, and human disease. *Annu. Rev. Biochem.* **75**, 333–366 (2006).
3. Barral, J.M., Broadley, S.A., Schaffar, G. & Hartl, F.U. Roles of molecular chaperones in protein misfolding diseases. *Semin. Cell Dev. Biol.* **15**, 17–29 (2004).
4. Bukau, B., Weissman, J. & Horwich, A. Molecular chaperones and protein quality control. *Cell* **125**, 443–451 (2006).
5. Mayer, M.P. Gymnastics of molecular chaperones. *Mol. Cell* **39**, 321–331 (2010).
6. Hipp, M.S., Park, S.H. & Hartl, F.U. Proteostasis impairment in protein-misfolding and -aggregation diseases. *Trends Cell Biol.* **24**, 506–514 (2014).
7. Landry, S.J. & Gierasch, L.M. Polypeptide interactions with molecular chaperones and their relationship to in vivo protein folding. *Annu. Rev. Biophys. Biomol. Struct.* **23**, 645–669 (1994).
8. Lindberg, I. *et al.* Chaperones in neurodegeneration. *J. Neurosci.* **35**, 13853–13859 (2015).
9. Schneider, C. *et al.* Pharmacologic shifting of a balance between protein refolding and degradation mediated by Hsp90. *Proc. Natl. Acad. Sci. USA* **93**, 14536–14541 (1996).
10. Jakob, U., Lilie, H., Meyer, I. & Buchner, J. Transient interaction of Hsp90 with early unfolding intermediates of citrate synthase. Implications for heat shock in vivo. *J. Biol. Chem.* **270**, 7288–7294 (1995).
11. Street, T.O., Lavery, L.A. & Agard, D.A. Substrate binding drives large-scale conformational changes in the Hsp90 molecular chaperone. *Mol. Cell* **42**, 96–105 (2011).
12. Dickey, C.A. *et al.* The high-affinity HSP90-CHIP complex recognizes and selectively degrades phosphorylated tau client proteins. *J. Clin. Invest.* **117**, 648–658 (2007).
13. Echeverria, P.C. & Picard, D. Molecular chaperones, essential partners of steroid hormone receptors for activity and mobility. *Biochim. Biophys. Acta* **1803**, 641–649 (2010).
14. Falsone, S.F., Kungl, A.J., Rek, A., Cappai, R. & Zangger, K. The molecular chaperone Hsp90 modulates intermediate steps of amyloid assembly of the Parkinson-related protein α-synuclein. *J. Biol. Chem.* **284**, 31190–31199 (2009).
15. Dekki, N. *et al.* Transthyretin binds to glucose-regulated proteins and is subjected to endocytosis by the pancreatic β-cell. *Cell. Mol. Life Sci.* **69**, 1733–1743 (2012).
16. Karagöz, G.E. *et al.* Hsp90-Tau complex reveals molecular basis for specificity in chaperone action. *Cell* **156**, 963–974 (2014).
17. Benson, M.D. & Uemichi, T. Transthyretin amyloidosis. *Amyloid* **3**, 44–56 (1996).
18. Sato, T. *et al.* Endoplasmic reticulum quality control regulates the fate of transthyretin variants in the cell. *EMBO J.* **26**, 2501–2512 (2007).
19. Chen, J.J. *et al.* Endoplasmic reticulum proteostasis influences the oligomeric state of an amyloidogenic protein secreted from mammalian cells. *Cell. Chem. Biol.* **23**, 1282–1293 (2016).
20. Planté-Bordeneuve, V. & Said, G. Transthyretin related familial amyloid polyneuropathy. *Curr. Opin. Neurol.* **13**, 569–573 (2000).
21. Connors, L.H., Lim, A., Prokaeva, T., Roskens, V.A. & Costello, C.E. Tabulation of human transthyretin (TTR) variants, 2003. *Amyloid* **10**, 160–184 (2003).
22. Bekircan-Kurt, C.E., Güneş, N., Yılmaz, A., Erdem-Özdamar, S. & Tan, E. Three Turkish families with different transthyretin mutations. *Neuromuscul. Disord.* **25**, 686–692 (2015).
23. Jiang, X. *et al.* An engineered transthyretin monomer that is nonamyloidogenic, unless it is partially denatured. *Biochemistry* **40**, 11442–11452 (2001).
24. Blake, C.C., Geisow, M.J., Swan, I.D., Rerat, C. & Rerat, B. Strjcture of human plasma prealbumin at 2-5 Å resolution. A preliminary report on the polypeptide chain conformation, quaternary structure and thyroxine binding. *J. Mol. Biol.* **88**, 1–12 (1974).
25. Johnson, S.M., Connelly, S., Fearns, C., Powers, E.T. & Kelly, J.W. The transthyretin amyloidoses: from delineating the molecular mechanism of aggregation linked to pathology to a regulatory-agency-approved drug. *J. Mol. Biol.* **421**, 185–203 (2012).
26. Reixach, N., Deechongkit, S., Jiang, X., Kelly, J.W. & Buxbaum, J.N. Tissue damage in the amyloidoses: transthyretin monomers and nonnative oligomers are the major cytotoxic species in tissue culture. *Proc. Natl. Acad. Sci. USA* **101**, 2817–2822 (2004).
27. Quintas, A., Saraiva, M.J. & Brito, R.M. The tetrameric protein transthyretin dissociates to a non-native monomer in solution. A novel model for amyloidogenesis. *J. Biol. Chem.* **274**, 32943–32949 (1999).
28. Lim, K.H. *et al.* Structural changes associated with transthyretin misfolding and amyloid formation revealed by solution and solid-state NMR. *Biochemistry* **55**, 1941–1944 (2016).
29. Lim, K.H., Dyson, H.J., Kelly, J.W. & Wright, P.E. Localized structural fluctuations promote amyloidogenic conformations in transthyretin. *J. Mol. Biol.* **425**, 977–988 (2013).
30. Bourgault, S. *et al.* Mechanisms of transthyretin cardiomyocyte toxicity inhibition by resveratrol analogs. *Biochem. Biophys. Res. Commun.* **410**, 707–713 (2011).
31. Neudecker, P. *et al.* Structure of an intermediate state in protein folding and aggregation. *Science* **336**, 362–366 (2012).
32. Sreedhar, A.S., Kalmár, E., Csermely, P. & Shen, Y.F. Hsp90 isoforms: functions, expression and clinical importance. *FEBS Lett.* **562**, 11–15 (2004).
33. Park, S.J., Borin, B.N., Martinez-Yamout, M.A. & Dyson, H.J. The client protein p53 adopts a molten globule-like state in the presence of Hsp90. *Nat. Struct. Mol. Biol.* **18**, 537–541 (2011).
34. Hagn, F. *et al.* Structural analysis of the interaction between Hsp90 and the tumor suppressor protein p53. *Nat. Struct. Mol. Biol.* **18**, 1086–1093 (2011).
35. Lorenz, O.R. *et al.* Modulation of the Hsp90 chaperone cycle by a stringent client protein. *Mol. Cell* **53**, 941–953 (2014).
36. Krukenberg, K.A., Förster, F., Rice, L.M., Sali, A. & Agard, D.A. Multiple conformations of *E. coli* Hsp90 in solution: insights into the conformational dynamics of Hsp90. *Structure* **16**, 755–765 (2008).
37. Karagöz, G.E. *et al.* N-terminal domain of human Hsp90 triggers binding to the cochaperone p23. *Proc. Natl. Acad. Sci. USA* **108**, 580–585 (2011).
38. Rosenzweig, R. & Kay, L.E. Bringing dynamic molecular machines into focus by methyl-TROSY NMR. *Annu. Rev. Biochem.* **83**, 291–315 (2014).
39. Liu, W.M. *et al.* A pH-sensitive, colorful, lanthanide-chelating paramagnetic NMR probe. *J. Am. Chem. Soc.* **134**, 17306–17313 (2012).
40. Keizers, P.H., Saragliadis, A., Hiruma, Y., Overhand, M. & Ubbink, M. Design, synthesis, and evaluation of a lanthanide chelating protein probe: CLaNP-5 yields predictable paramagnetic effects independent of environment. *J. Am. Chem. Soc.* **130**, 14802–14812 (2008).
41. Pintacuda, G., John, M., Su, X.C. & Otting, G. NMR structure determination of protein-ligand complexes by lanthanide labeling. *Acc. Chem. Res.* **40**, 206–212 (2007).
42. Keizers, P.H. & Ubbink, M. Paramagnetic tagging for protein structure and dynamics analysis. *Prog. Nucl. Magn. Reson. Spectrosc.* **58**, 88–96 (2011).
43. Jackson, S.E. Hsp90: structure and function. *Top. Curr. Chem.* **328**, 155–240 (2013).
44. Vaughan, C.K. *et al.* Structure of an Hsp90-Cdc37-Cdk4 complex. *Mol. Cell* **23**, 697–707 (2006).
45. Chakraborty, R., Muchtar, E. & Gertz, M.A. Newer therapies for amyloid cardiomyopathy. *Curr. Heart Fail. Rep.* **13**, 237–246 (2016).
46. Verba, K.A. *et al.* Atomic structure of Hsp90-Cdc37-Cdk4 reveals that Hsp90 traps and stabilizes an unfolded kinase. *Science* **352**, 1542–1547 (2016).
47. Meyer, P. *et al.* Structural basis for recruitment of the ATPase activator Aha1 to the Hsp90 chaperone machinery. *EMBO J.* **23**, 511–519 (2004).
48. Ali, M.M. *et al.* Crystal structure of an Hsp90-nucleotide-p23/Sba1 closed chaperone complex. *Nature* **440**, 1013–1017 (2006).
49. Zhang, M., Kadota, Y., Prodromou, C., Shirasu, K. & Pearl, L.H. Structural basis for assembly of Hsp90-Sgt1-CHORD protein complexes: implications for chaperoning of NLR innate immunity receptors. *Mol. Cell* **39**, 269–281 (2010).
50. Carman, A., Kishinevsky, S., Koren, J. III, Lou, W. & Chiosis, G. Chaperone-dependent neurodegeneration: a molecular perspective on therapeutic intervention. *J. Alzheimers Dis. Parkinsonism* **2013**, 007 (2013).
51. Liu, K., Kelly, J.W. & Wemmer, D.E. Native state hydrogen exchange study of suppressor and pathogenic variants of transthyretin. *J. Mol. Biol.* **320**, 821–832 (2002).

ONLINE METHODS

Protein preparation. We cloned human wild-type TTR into a pQE30 vector (Qiagen) and used it as a template to generate M-TTR (including the mutations F87M and L110M) and M-TTR/M13C. Proteins were expressed in the M15 *Escherichia coli* strain. For uniform ^{13}C-^{15}N isotopic labeling, cells were grown in M9 minimal medium with $^{15}NH_4Cl$ and [D-^{13}C]-glucose as the sole sources of nitrogen and carbon, respectively. We used 2-oxo-3[D_2]-4[^{13}C]-butyrate and 2-hydroxy-2-[D_3]methyl-3-oxo-[2,4-$^{13}C_2$]-butanoic acid (NMR Bio) as precursors for the selective [^1H-^{13}C]-labeling of isoleucine δ_1 and leucine δ and valine γ methyl groups in fully deuterated media, respectively[52]. Cells were lysed by sonication, and recombinant proteins were purified by anion-exchange chromatography (using HiTrap Q FF columns (GE Healthcare)) with 20 mM sodium phosphate, 5 mM EDTA, pH 9.5, as binding buffer, with 500 mM NaCl included in the elution buffer. We subsequently purified proteins by size-exclusion chromatography using a Superdex 75 column (GE Healthcare) in 20 mM sodium phosphate, 150 mM NaCl, 5 mM EDTA, pH 9.5. Proteins were further purified by reverse-phase chromatography using a pre-packed C8 column (Higgins Analytical). Binding buffer consisted of 5% acetonitrile, 0.1% trifluoroacetic acid, and the elution buffer was 95% acetonitrile, 0.1% trifluoroacetic acid. Pure protein was lyophilized and, after resuspension, dialyzed against 50 mM MES, 100 mM NaCl, 5 mM EDTA, 5 mM DTT, pH 6.5, for NMR spectroscopy studies.

For the tagging of M-TTR/M13C with CLaNP-7 lanthanide tags (with either Tm^{3+} paramagnetic or Lu^{3+} diamagnetic ions), pure unlabeled M-TTR was dialyzed against 20 mM sodium phosphate, 150 mM NaCl, pH 7.2, and incubated for 2 h on ice with five equivalents of lanthanide per mole of protein. Sample was dialyzed overnight against the aforementioned buffer and subjected to size-exclusion purification using a Superdex 75 column (GE Healthcare) to get rid of unbound lanthanide. Spin-labeled M-TTR variants were finally dialyzed against 25 mM sodium phosphate, 300 mM NaCl, 1 mM DTT, pH 7.2, in 100% D_2O for NMR spectroscopy analysis.

Human Hsp90β (full-length as well as constructs containing only N-terminal and M domains or M domain alone) was cloned in pET28a (Novagen) and expressed in the Rosetta 2 (DE3) *E. coli* strain. Perdeuterated Hsp90 (full-length and N-terminal–M-domain construct), which was selectively protonated at isoleucine δ_1 methyl groups, was produced in 99% D_2O M9 minimal media with $^{15}NH_4Cl$ and [^2H,^{13}C]-glucose as the sole sources of nitrogen and carbon, respectively. We used 2-oxo-3[D_2]-4[^{13}C]-butyrate (NMR-Bio) as a metabolic precursor for the selective [^1H-^{13}C]-labeling of isoleucine δ_1 methyl groups in an otherwise [^{15}N,^{12}C,^2H] protein[52]. For uniform ^{13}C-^{15}N isotopic labeling of Hsp90 M-domain mutants for assignment, cells were grown in M9 minimal medium with $^{15}NH_4Cl$ and [D-^{13}C]-glucose as the sole sources of nitrogen and carbon, respectively. Overexpressed recombinant protein was purified by Ni^{2+}-affinity chromatography using Ni^{2+}-NTA agarose (Qiagen) followed by size-exclusion chromatography (Superdex 200; GE Healthcare) in 10 mM HEPES, 500 mM KCl, 1 mM DTT, pH 7.5. Fractions containing pure protein were pooled and extensively dialyzed against 25 mM sodium phosphate, 300 mM NaCl, 1 mM DTT, pH 7.2, in 100% D_2O for NMR spectroscopy analysis. N-terminal–M- and M-domain constructs of Hsp90 remained monomeric in solution. Samples destined for SAXS analysis (produced in regular LB media) were dialyzed against 25 mM HEPES, 10 mM KCl, 5 mM $MgCl_2$, 1 mM DTT, pH 7.4. Pure Hsp90 proteins were kept at concentrations ≤ 0.25 mM to prevent the formation of higher-order oligomers.

NMR spectroscopy. For resonance assignment and structure determination, M-TTR sample concentrations were in the range of 0.6–0.8 mM and the temperature was set to 25 °C. To decrease conformational exchange contributions in M-TTR[29] and obtain high-resolution 3D spectra, we acquired triple-resonance and NOESY experiments at a hydrostatic pressure of 500 bar using a commercial pressure device (Daedalus Innovations LLC, PA) attached to a 700-MHz NMR spectrometer (Bruker) equipped with a cryogenic HCN probe. When we increased the pressure to 500 bar, the position of NMR signals remained largely unchanged, whereas line broadening decreased. Residue-specific backbone and side chain resonance assignment was then achieved by 3D HNCA, HNCOCA, HNCO[53,54], (H)CCH-TOCSY[55], ^{15}N NOESY-HSQC and ^{13}C NOESY-HSQC (both aliphatic and aromatic) experiments[56,57]. NOESY experiments were run with 120 ms of mixing time. Spectra were processed using TopSpin (Bruker) and NMRPipe[58] and analyzed in SPARKY (Goddard & Kneller, UCSF). We submitted experimentally derived chemical shifts to TALOS-N[59] to obtain S^2 backbone order parameters as described in ref. 60. Cross-peaks in 3D ^{15}N-NOESY-HSQC and 3D ^{13}C-NOESY-HSQC spectra of M-TTR were manually picked, and CYANA 3.0 (ref. 61) was used to assign them, generate distance constraints, and calculate initial structural models. We used the TALOS-N[59] software to obtain backbone dihedral angle (φ and ψ) constraints. After an initial structure calculation, we manually inspected all cross-peak assignments of the NOESY spectra to re-pick peaks and modify assignments when necessary. For the final calculations, 50 hydrogen-bond restraints based on characteristic NOE contacts were added. We checked the quality of the final structure with the Protein Structure Validation Software Suite[62]. Structures were displayed using PyMOL (Schroedinger, LCC).

To probe the interaction with Hsp90, we recorded two-dimensional ^1H-^{15}N correlation spectra of wild-type TTR and M-TTR (150 μM protein concentration) at ambient pressure in the absence and presence of an equimolar concentration of Hsp90. Because wild-type TTR is a 55-kDa homotetramer, we recorded ^1H-^{15}N TROSY spectra at 900 MHz on ^2H/^{15}N-labeled TTR, whereas we acquired ^1H-^{15}N HSQC spectra for ^{13}C/^{15}N-labeled M-TTR at 600 MHz.

^1H-^{13}C methyl-TROSY[63] spectra of Hsp90 were acquired at 25 °C (ambient pressure) on Bruker Avance III 800 MHz and Avance 900 MHz spectrometers (both equipped with TCI cryoprobes). We obtained PCSs by comparing the spectrum of a 30 μM isoleucine-labeled Hsp90 protein solution with 0.5 molar equivalents of Tm^{3+}-CLaNP7-tagged M-TTR/M13C (paramagnetic) with that containing the same ratio of Lu^{3+}-CLaNP7-tagged M-TTR/M13C (diamagnetic).

We confirmed previously available assignments of Hsp90 isoleucine methyl groups[16,37] and extended them through site-directed mutagenesis of specific isoleucine residues both in full-length Hsp90 and in isolated N-terminal–M and M domains. Substituting a single isoleucine residue for valine will lead to an NMR spectrum in which one isoleucine resonance will disappear, thus enabling the assignment of the specific mutated residue. The following mutations were prepared: I37V, I104V, I145V, I579V, I627V, I689V and I707V (in full-length Hsp90); I53V, I72V, I75V, I98V, I181V, I212V, I224V, I249V and I271V (in Hsp90 N-terminal–M-domain construct); and I276V, I295V, I352V, I361V, I376V, I389V, I399V, I403V, I485V and I516V (in Hsp90 M-domain construct). ^1H-^{13}C methyl-TROSY[63] spectra were acquired at 25 °C on Bruker Avance III 800 MHz and Avance 900 MHz spectrometers for mutants based on full-length and N-terminal–M-domain constructs. For mutants based on Hsp90's M domain, ^{13}C-HSQC experiments were acquired at 35 °C on Bruker Avance III 800 MHz, Avance III 700 MHz and Avance III 600 MHz spectrometers (all equipped with TCI cryoprobes). In addition, [^1H-^{15}N]-HSQC, [^1H-^{13}C]-HSQC, 3D HNCO, 3D HNCACB, 3D HNCOCA, 3D HcCH-TOCSY (15-ms mixing time), 3D ^{15}N-[^1H-^1H]-NOESY (80-ms mixing time) and 3D ^{13}C-[^1H-^1H]-NOESY (80-ms mixing time) NMR spectroscopy experiments were used on ^{15}N-^{13}C- and ^2H-^{15}N-^{13}C-uniformly labeled M-domain samples. To further validate the resonance assignments, we carried out 3D ^{13}C-[^1H-^1H]-NOESY and 4D ^1H-[^{13}C-^{13}C]-^1H-NOESY experiments (both with 200-ms mixing times) for full-length Hsp90 at 35 °C on Bruker Avance III 950 MHz and Avance 900 MHz spectrometers (both equipped with TCI cryoprobes). Spectra were processed and Fourier-transformed in TopSpin and analyzed in Sparky (Goddard & Kneller, UCSF) and ccpnmr Analysis 2.2.1 (ref. 64). Out of 48 isoleucine residues present in full-length Hsp90, 44 were sequence-specifically assigned (38 out of 38 excluding the C-terminal domain).

Isothermal titration calorimetry. ITC was carried out with an ITC-200 (Microcal) at a constant temperature (25 °C) in 25 mM sodium phosphate, 150 mM NaCl, 1 mM DTT, pH 7.2. Deionized water was used in the reference cell. All solutions were thoroughly degassed before use. We determined the reproducibility of the measurements by using replicates of the independent measurements and different molar ratios. The sample cell (~200 μl) contained Hsp90 ranging from 22.75 to 30 μM, and the M-TTR titrating solution ranged from 166.5 to 1671 μM. At each titration step, a 0.2-μl injection was followed by 25 injections of 1.5 μl each into the sample cell, with a stirring speed of 500 r.p.m. and intervals of 180 s between injections. We obtained heats due to dilution by titrating M-TTR into buffer, and subtracted them from all the corresponding curves shown in the main text and **Supplementary Figure 2**. The data were fitted using Microcal software. We obtained thermodynamic parameters by fitting a macroscopic binding model allowing for two sets of binding sites.

Small-angle X-ray scattering. SAXS data were collected at 25 °C from pure and monodisperse samples of Hsp90, M-TTR and Hsp90–M-TTR complex at a 2:1

doi:10.1038/nsmb.3380

molar ratio (i.e., one M-TTR molecule per Hsp90 dimer). Sample concentrations ranged from 20 to 100 μM in 25 mM HEPES, 10 mM KCl, 5 mM $MgCl_2$, 1 mM DTT, pH 7.4, in the absence or presence of 1 mM ADP. $P(r)$ distributions correspond to a 50 μM solution of Hsp90. The scattering profiles were analyzed using the ATSAS package[65] and standard procedures. Assuming only the lowest observed affinity (47.3 μM), 70% of the Hsp90 dimer would be bound to M-TTR in the presented SAXS curves.

Data availability. Chemical shifts of M-TTR have been deposited in the Biological Magnetic Resonance Bank (BMRB) under accession number 25986. The coordinates for the 3D structure of M-TTR have been deposited in the Protein Data Bank with accession number 2NBO. Other data generated and/or analyzed in the current study are available from the corresponding author upon reasonable request.

52. Tugarinov, V., Kanelis, V. & Kay, L.E. Isotope labeling strategies for the study of high-molecular-weight proteins by solution NMR spectroscopy. *Nat. Protoc.* **1**, 749–754 (2006).
53. Bax, A. Multidimensional nuclear-magnetic-resonance methods for protein studies. *Curr. Opin. Struct. Biol.* **4**, 738–744 (1994).
54. Sattler, M., Schleucher, J. & Griesinger, C. Heteronuclear multidimensional NMR experiments for the structure determination of proteins in solution employing pulsed field gradients. *Prog. Nucl. Magn. Reson. Spectrosc.* **34**, 93–158 (1999).
55. Bax, A., Clore, G.M. & Gronenborn, A.M. H-1-H-1 correlation via isotropic mixing of C-13 magnetization, a new 3-dimensional approach for assigning H-1 and C-13 spectra of C-13-enriched proteins. *J. Magn. Reson.* **88**, 425–431 (1990).
56. Wuthrich, K. *NMR of Proteins and Nucleic Acids* (Wiley Interscience, 1986).
57. Marion, D. *et al.* Overcoming the overlap problem in the assignment of 1H NMR spectra of larger proteins by use of three-dimensional heteronuclear 1H-15N Hartmann-Hahn-multiple quantum coherence and nuclear Overhauser-multiple quantum coherence spectroscopy: application to interleukin 1 beta. *Biochemistry* **28**, 6150–6156 (1989).
58. Delaglio, F. *et al.* NMRPipe: a multidimensional spectral processing system based on UNIX pipes. *J. Biomol. NMR* **6**, 277–293 (1995).
59. Shen, Y. & Bax, A. Protein backbone and sidechain torsion angles predicted from NMR chemical shifts using artificial neural networks. *J. Biomol. NMR* **56**, 227–241 (2013).
60. Berjanskii, M.V. & Wishart, D.S. A simple method to predict protein flexibility using secondary chemical shifts. *J. Am. Chem. Soc.* **127**, 14970–14971 (2005).
61. Güntert, P. Automated NMR structure calculation with CYANA. *Methods Mol. Biol.* **278**, 353–378 (2004).
62. Bhattacharya, A., Tejero, R. & Montelione, G.T. Evaluating protein structures determined by structural genomics consortia. *Proteins* **66**, 778–795 (2007).
63. Tugarinov, V., Hwang, P.M. & Kay, L.E. Nuclear magnetic resonance spectroscopy of high-molecular-weight proteins. *Annu. Rev. Biochem.* **73**, 107–146 (2004).
64. Vranken, W.F. *et al.* The CCPN data model for NMR spectroscopy: development of a software pipeline. *Proteins* **59**, 687–696 (2005).
65. Petoukhov, M.V. *et al.* New developments in the ATSAS program package for small-angle scattering data analysis. *J. Appl. Crystallogr.* **45**, 342–350 (2012).

Erratum: Mechanistic basis for the recognition of a misfolded protein by the molecular chaperone Hsp90

Javier Oroz, Jin Hae Kim, Bliss J Chang & Markus Zweckstetter
***Nat. Struct. Mol. Biol.* doi:10.1038/nsmb.3380; corrected online 13 March 2017**

In the version of this article initially published online, there was an error in the *y*-axis label of Figure 1e. The error has been corrected in the print, PDF and HTML versions of this article.